



Halo of ice deformation observed over the Maud Rise seamount

R. W. Lindsay,¹ R. Kwok,² L. de Steur,³ and W. Meier⁴

Received 8 May 2008; revised 13 June 2008; accepted 30 June 2008; published 6 August 2008.

[1] A distinctive halo of sea ice deformation was observed above the Maud Rise seamount in the eastern Weddell Sea in the winter of 2005. The deformation halo is coincident with a halo of low mean ice concentration that is often observed in the region. Monthly mean ice vorticity estimates for the months July through November reveal the deformation zone most clearly in an arc about 100 km northwest of the seamount where there is a strong gradient in the bathymetry at depths of 3000–5000 m. The deformation was computed from satellite-based ice motion vectors derived from Envisat Synthetic Aperture Radar backscatter images. The deformation halo is evidence of a Taylor cap circulation over the seamount, which has been described and analyzed with modeling studies and concurrent oceanographic observations obtained during an extensive field campaign. **Citation:** Lindsay, R. W., R. Kwok, L. de Steur, and W. Meier (2008), Halo of ice deformation observed over the Maud Rise seamount, *Geophys. Res. Lett.*, 35, L15501, doi:10.1029/2008GL034629.

1. Introduction

[2] The Maud Rise seamount in the eastern Weddell Sea rises from the abyssal plain at 5000 m depth to within 1700 m of the surface. It is located about 500 km north of the Antarctic continent at 65°S, 2.5°E. Here sea ice forms every winter to an extent of about 1500 km north of the coast and usually melts back to near the coast every summer. The region around Maud Rise has attracted research attention because of the very low static stability of the ocean to great depths, the large surface heat fluxes observed in the region, and the likely occurrence of deep convection and ventilation events for the abyssal ocean waters [e.g., *Martinson et al.*, 1981; *McPhee et al.*, 1996; *Muench et al.*, 2001].

[3] The existence of a persistent halo of low mean ice concentration centered on the seamount was first described by *Lindsay et al.* [2004]. The mean was computed from satellite-based passive-microwave measurements over a 23-year period and the 300-km circular halo is evident most clearly in the months July through November. It is most distinct in October; even then, however, the mean ice concentration in the halo is just 10% less than in the center, where it is very near 100%.

[4] The mean motion of the ice in this region is to the north. It was unknown whether the seamount modifies this

motion in any way and, in particular, if the observed halo of low ice concentration is induced dynamically by ice divergence or is a feature of increased ocean heat flux from below. Is the ice deformed in a consistent manner that might aid or diminish the rate of ice formation and hence modify the static stability of the upper water column?

[5] In the austral winter of 2005 a winter field campaign, called MaudNESS, was mounted to investigate the role of nonlinearities in the equation of state of sea water in initiating and maintaining deep convective overturning in the open Southern Ocean. One such nonlinearity is the thermobaric effect, the pressure dependence of the thermal expansion factor for seawater. The project consisted of a late-winter research cruise to the Weddell Sea that obtained a full array of oceanographic observations and a variety of modeling activities covering a wide range of spatial scales [*McPhee and the MaudNESS Science Group*, 2006; *Shaw et al.*, 2006; *De Steur et al.*, 2007]. To supplement the in situ observations, high-resolution satellite-based observations of the ice motion were obtained during the field campaign to determine if the seamount has a direct influence on the ice motion and deformation in the region.

2. Observations

2.1. AMSR Ice Concentration

[6] Daily near-real-time Advanced Microwave Scanning Radiometer for EOS (AMSR-E) ice concentration estimates were obtained from the University of Bremen [*Spreen et al.*, 2007]. They are based on the 89-GHz channel using their Arctic Radiation and Turbulence Interaction Study Sea Ice algorithm and have a spatial resolution of 6.25 km.

2.2. AMSR Ice Motion

[7] The mean motion in the region was obtained from tracking ice in pairs of daily images of the 36-GHz and 89-GHz horizontally-polarized near-real-time brightness temperatures [*Cavalieri and Comiso*, 2004a, 2004b] using a cross-correlation method [e.g., *Kwok et al.*, 1998]. The motion fields from the two channels were combined onto a 31-km grid using optimal interpolation [*Meier et al.*, 2000]. The accuracy of the ice tracking is estimated at 3–4 km day⁻¹ (RMS error) for each velocity component with small biases, based on comparisons with Arctic buoys [*Meier and Dai*, 2006]; because of the more dynamic nature of southern hemisphere sea ice, errors are slightly higher in the Antarctic. The low accuracy of the tracking precludes the use of these data for determining detailed ice deformation, but the frequent temporal and broad spatial coverage make these data very useful for determining the mean motion.

2.3. Envisat Ice Motion

[8] A set of Wide Swath VV Medium Resolution backscatter images centered on the Maud Rise seamount were

¹Polar Science Center, Applied Physics Laboratory, University of Washington, Seattle, Washington, USA.

²Jet Propulsion Laboratory, California Institute of Technology, Pasadena, California, USA.

³Norwegian Polar Institute, Tromsø, Norway.

⁴National Snow and Ice Data Center, University of Colorado, Boulder, Colorado, USA.

acquired with the cooperation of the European Space Agency. Each image measures 400×400 km and has a geometric resolution of 150 m. The ice tracking between image pairs was performed by the RadarSat Geophysical Processing System (RGPS) [Kwok, 2002] at the Jet Propulsion Laboratory. A total of 42 image pairs are utilized for the tracking in the time period 2 July–10 September 2005. The displacement vectors are determined on a 10-km grid; the time interval between the pairs ranges between 0.34 and 3.64 days. When compared to buoy motion, the accuracy of the ice tracking is on the order of one pixel, in this case 150 m [Lindsay and Stern, 2003]. The ice deformation is determined from strain rate determinations for each 10-km cell by computing the line integral of the velocity components around each cell. The tracking errors give rise to error standard deviations of $0.5\% \text{ day}^{-1}$ in the divergence, shear, and vorticity. The uncertainty in the area change of a cell is 1.4% due to tracking errors and 3.2% due to resolving the cell boundary with only four points [Lindsay and Stern, 2003].

3. Results

[9] The mean ice concentration in the vicinity of the Maud Rise seamount for the three-month period 2 July–10 September 2005 is reduced primarily in an arc extending from the north, through the west, and then to the southeast of the seamount (Figure 1a). The mean concentration in the arc is just 10% less than the near complete coverage over the seamount itself but it is well defined in the northwestern quadrant. The mean motion of the ice during this time period is in a cyclonic curve from the southeast to the northwest (Figure 1b), with the motion predominantly from the south near the summit of the seamount. The patterns of both the ice concentration and the mean ice motion are similar to those of the long-term means [Lindsay et al., 2004].

[10] Mean vorticity observations over the period reveal the pattern of ice deformation most clearly (Figure 2). An arc of positive vorticity (anticyclonic flow) extends from the north, west, and southeast in a pattern that is very similar to what is seen in the mean ice concentration for the period, although to the south it is slightly less well defined. The vorticity maximum is closely aligned with a region of the seamount where the bathymetric gradient is very steep and the depths range from 3000 to 5000 m. Maps of both the mean divergence and the variability of the divergence (not shown) do not exhibit this spatial pattern. The vorticity within the arc is almost always positive during the period but it is not well correlated with the ice speed.

[11] Figure 3 shows a time series of the ice speed and vorticity observations in the northwest quadrant of the arc where the mean vorticity is large, above 0.05 day^{-1} . It shows the duration of each of the deformation estimates in this region. Both the speed and the vorticity vary considerably during the period, but the vorticity in this region is almost always positive. The divergence of the ice pack, which might have explained some of the low ice concentrations, is consistently small in the same region and is both positive and negative (not shown). It does not appear that ice divergence was an important factor in the formation of the low-ice concentration halo.

[12] The mean relative vorticity of the ocean (Figure 4) is simulated in a 180-day model run performed with Miami

Isopycnic Coordinate Ocean Model (MICOM) [Bleck and Boudra, 1981] using 11 layers in the vertical, 0.1° in the horizontal, and an imposed barotropic westward flow of 1.5 cm s^{-1} . Model parameters are chosen to be identical to those described by De Steur et al. [2007]. Averaged over the last 140 days, neglecting possible spin-up effects, the maximum mean vorticity is situated above the steepest parts of the northern flank of Maud Rise, as in the observations. The model simulations show that the band of positive vorticity observed in the ice movement is likely the result of the mean oceanic flow around the seamount inducing a displaced Taylor cap with maximum anticyclonic motion above the steep bathymetry of the seamount. A similar result is found by Beckmann et al. [2001] in numerical experiments with a coupled ice-ocean model that includes tidal effects.

4. Discussion

[13] Hydrographic observations have established that the ocean circulation of the region is affected by the presence of the seamount (see, e.g., Muench et al. [2001] for an overview). The generic temperature profile in the region consists of a surface (~ 0 –100 m) layer of cooler, fresher water, overlying a warmer saltier layer (~ 100 –500 m), which in turn overlies a much thicker, cooler layer. In the region of Maud Rise, anomalously warm waters are found over the flanks of the rise, with a colder cap of water overlying the top of the rise, [e.g., Gordon, 1978; Bersch et al., 1992; Muench et al., 2001]. This warm “halo” layer [Muench et al., 2001] is a candidate heat source for thinning of the ice cover and several authors [e.g., Martinson et al., 1981; McPhee et al., 1999; Muench et al., 2001] consider strong vertical heat fluxes near the surface.

[14] Theoretical considerations [e.g., Ou, 1991] indicate that, given the physical parameters of the system (the dimensions of Maud Rise, the ambient ocean stratification, and the measured speeds of flow), Taylor cap dynamics are important, i.e., the ocean flow intensifies around the flanks of the seamount; a quasi-trapped, anticyclonic circulation (with associated doming of isopycnals) is found in the region; and a relatively stagnant cap of water forms directly above the seamount. Maud Rise is not the only location where a Taylor cap or column influences sea ice. Martin and Drucker [1997] report a Taylor column in the spring sea ice concentration over the shallow (30 m) Herald Shoal in the Chukchi Sea in the Arctic.

[15] Several authors hypothesize how environmental features may interact to cause ice thinning and polynya formation. Holland [2001a, 2001b] uses an isopycnal model to demonstrate how Ekman effects, induced by ocean circulation (in particular, cyclonic eddy shedding) can lead to ice thinning and polynya formation around an idealized seamount. He shows that transients in the mean oceanic flow toward the seamount produce polynya positioned on the flank of the seamount and located about 90 degrees to the left of the direction of the oncoming flow transient. Beckmann et al. [2001] use a coupled sea-ice-ocean model to simulate the response to steady and tidal flows around a simulation of Maud Rise to demonstrate substantial tidal amplification around the seamount. They predict polynya formation in the northwest quadrant of the rise driven dominantly by rectified tidal effects, the non-tidal

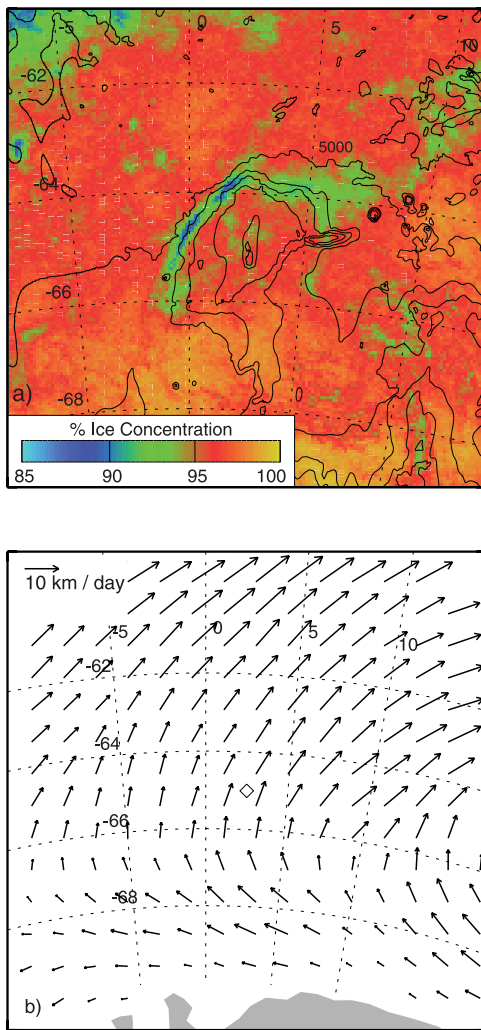


Figure 1. (a) Mean ice concentration, 2 July–10 September 2005, from daily AMSR passive microwave brightness temperatures. The contours indicate the topography of the seamount (contour interval 700 m). Data are from the University of Bremen, Bremen, Germany. (b) Mean ice motion over the same time interval from ice tracking using AMSR-E microwave brightness temperature images. The summit of the Maud Rise seamount is marked with a diamond. Data are from the National Snow and Ice Data Center, University of Colorado, Boulder, Colorado, USA.

mean-flow being required only to separate the polynya from the rise. The potential for tidal flows to enhance vertical motion and mixing is also investigated more idealistically by *Goldner and Chapman* [1997]. In addition, *McPhee* [2003] shows how thermobaricity can be an important mechanism in stimulating or enhancing convective mixing under the conditions found near Maud Rise. Despite these many studies, consensus has not yet been reached concerning either the dominant mechanism causing ice thinning or the region relative to the seamount most favored for thinning.

[16] Regional hydrographic and current observations from the 2005 MaudNESS winter field campaign in the Maud Rise seamount region show that an annular halo consisting largely of warm deep water encircled the rise at

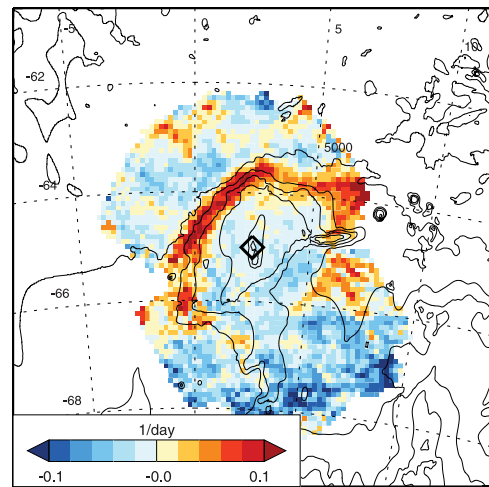


Figure 2. The mean vorticity of the ice velocity for the period 2 July–10 September 2005. At least five observations were obtained for each location and the mean is weighted by the time interval of each observation.

depths just below the mixed layer [*De Steur et al.*, 2007]. The halo was associated with elevated isopycnals and, on the northern flank of the rise, strong subsurface velocities up to 20 cm s^{-1} . Intercomparison of these observations with winter 1986 and 1994 conditions confirms the presence of the halo and suggests that it, and associated warm pools west of the rise, is at least semipermanent features of the region. These observational results compare well with the output from an isopycnic ocean model for a variety of parameters including shape of the seamount, inflow conditions, and vertical stratification [*De Steur et al.*, 2007]. The model captures processes associated with a steady westward flow impinging on the isolated seamount and

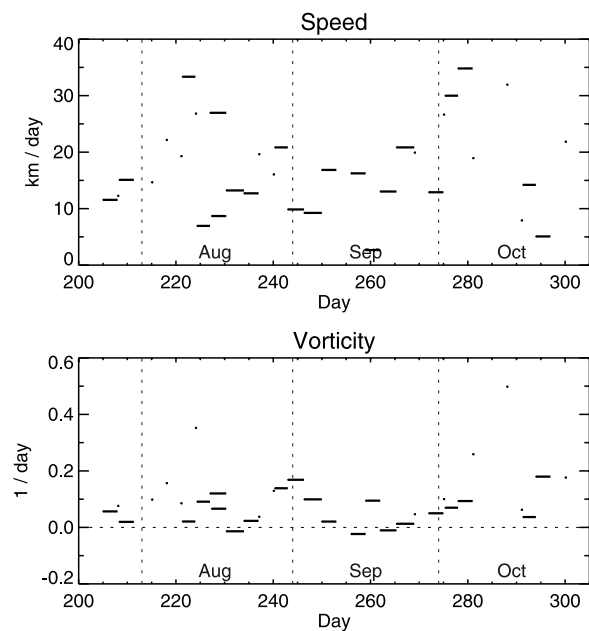


Figure 3. Time series of the ice speed and vorticity for the northwest portion of the vorticity arc where the mean vorticity exceeds 0.07 day^{-1} . Lines indicate the time interval for each set of ice displacement observations.

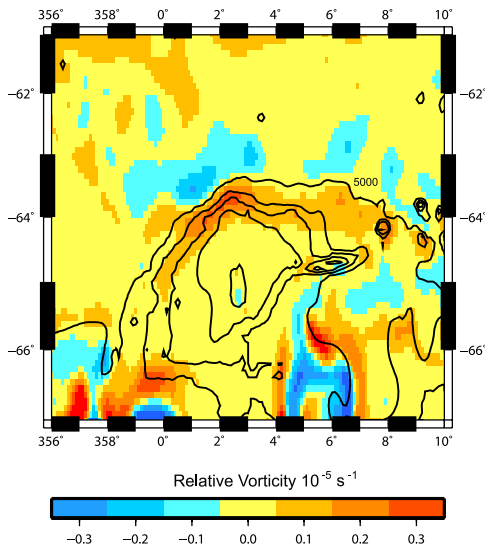


Figure 4. Mean relative vorticity of the MICOM model flow for the top layer, 100 m thick, for an inflow velocity of 1.5 cm s^{-1} . The contours indicate the topography of the seamount (contour interval 700 m).

shows (1) that the dynamics of the warm-water halo with a shallow mixed layer are related to the formation of a jet surrounding the rise and the overlying Taylor column and (2) that eddies of alternating sign (cyclones and anticyclones) are formed from instability of the jet-like flow structure, and are subsequently shed from the western flanks of the rise.

[17] Despite the formation of these transient eddies slightly west-northwest of the seamount, the time-mean relative vorticity in the halo in the upper ocean that closely wraps around the seamount is anticyclonic (Figure 4). This feature is in excellent agreement with the observed positive vorticity in sea ice velocity (Figure 2). To answer our initial question of whether the ice deformation is causing the reduction of sea ice concentration in the halo, we conclude that the semipermanent feature of the jet and warm-water halo surrounding Maud Rise is a likely candidate for causing both of the coincident bands of high vorticity and low ice concentration. The oceanic jet and band of anticyclonic vorticity induces deformation in the sea ice cover and the heat flux from the underlying Warm Deep Water maintains an area of relatively low ice concentration. The ice deformation itself does not appear to be the cause of the low ice concentration near the seamount since the divergence is negligible.

[18] **Acknowledgments.** This research is supported by the National Science Foundation Office of Polar Programs under grant OPP 0337751. The Envisat SAR images were acquired through the help of the European Space Agency.

References

- Beckmann, A., R. Timmermann, A. F. Pereira, and C. Mohn (2001), The effect of flow at Maud Rise on the sea-ice cover: Numerical experiments, *Ocean Dyn.*, *52*, 11–25.
- Bersch, M., G. A. Becker, H. Frey, and K. P. Koltermann (1992), Topographic effects of the Maud Rise on the stratification and circulation of the Weddell Gyre, *Deep Sea Res.*, *39*, 303–331.
- Bleck, R., and D. B. Boudra (1981), Initial testing of a numerical ocean circulation model using a hybrid (quasi-isopycnic) vertical coordinate, *J. Phys. Oceanogr.*, *11*, 755–770.
- Cavalieri, D., and J. Comiso (2004a), AMSR-E/Aqua Daily L3 6.25 km 89 GHz Brightness Temperature (Tb) Polar Grids V001, http://nsidc.org/data/ae_si6.html, Natl. Snow and Ice Data Cent., Boulder, Colo.
- Cavalieri, D., and J. Comiso (2004b), AMSR-E/Aqua daily L3 12.5 km Tb, Sea Ice Conc., & Snow Depth Polar Grids V001, http://nsidc.org/data/ae_si12.html, Natl. Snow and Ice Data Cent., Boulder, Colo.
- De Steur, L., D. M. Holland, R. Muench, and M. G. McPhee (2007), The warm-water 'halo' around Maud Rise: Properties, dynamics and impact, *Deep Sea Res., Part I*, *54*, 871–896.
- Drinkwater, M. (1998), *ERS-1/2 Synthetic Aperture Data*, Jet Propul. Lab., Pasadena, Calif.
- Goldner, D. R., and D. C. Chapman (1997), Flow and particle motion induced above a tall seamount by steady and tidal background currents, *Deep Sea Res., Part I*, *44*, 719–744.
- Gordon, L. (1978), Deep Antarctic convection west of Maud Rise, *J. Phys. Oceanogr.*, *8*, 600–612.
- Gordon, L. (1991), Two stable modes of Southern Ocean winter stratification, in *Deep Convection and Deep Water Formation in the Oceans*, edited by P.-C. Chu and J.-C. Gascard, *Elsevier Oceanogr. Ser.*, *57*, 17–35.
- Holland, D. M. (2001a), Explaining the Weddell Polynya: A large ocean eddy shed at Maud Rise, *Science*, *292*, 1697–1700.
- Holland, D. M. (2001b), Transient sea-ice polynya forced by environmental flow variability, *Prog. Oceanogr.*, *48*, 475–532.
- Kwok, R. (1998), The RADARSAT Geophysical Processor System, in *Analysis of SAR Data of the Polar Oceans*, edited by C. Tsatsoulis and R. Kwok, pp. 235–257, Springer, New York.
- Kwok, R. (2002), Sea ice concentration estimates from satellite passive microwave radiometry and openings from SAR ice motion, *Geophys. Res. Lett.*, *29*(9), 1311, doi:10.1029/2002GL014787.
- Kwok, R., A. Schweiger, D. A. Rothrock, S. Pang, and C. Kottmeier (1998), Sea ice motion from satellite passive microwave imagery assessed with ERS SAR and buoy motions, *J. Geophys. Res.*, *103*, 8191–8214.
- Lindsay, R. W., and H. Stern (2003), The RadarSat Geophysical Processor System: Quality of sea ice trajectory and deformation estimates, *J. Atmos. Ocean. Technol.*, *20*, 1333–1347.
- Lindsay, R. W., D. M. Holland, and R. A. Woodgate (2004), Halo of low ice concentration observed over the Maud Rise Seamount, *Geophys. Res. Lett.*, *31*, L13302, doi:10.1029/2004GL019831.
- Martin, S., and R. Drucker (1997), The effect of possible Taylor columns on the summer ice retreat in the Chukchi Sea, *J. Geophys. Res.*, *102*, 10,473–10,482.
- Martinson, D. G., P. D. Killworth, and A. L. Gordon (1981), A convective model for the Weddell Polynya, *J. Phys. Oceanogr.*, *11*, 466–488.
- McPhee, M. G. (2003), Is thermobaricity a major factor in Southern Ocean ventilation?, *Antarct. Sci.*, *15*, 153–160.
- McPhee, M. G., and the MaudNESS Science Group (2006), The Maud Rise Nonlinear Equation of State Study (MaudNESS) in the eastern Weddell Sea, Antarctica, *Eos Trans. AGU*, *87*(36), Ocean Sci. Meet. Suppl., Abstract OS46B-01.
- McPhee, M. G., S. F. Ackley, P. Guest, B. A. Huber, D. G. Martinson, J. H. Morison, R. D. Muench, L. Padman, and T. P. Stanton (1996), The Antarctic Flux Zone Experiment, *Bull. Am. Meteorol. Soc.*, *77*, 1221–1232.
- McPhee, M. G., C. Kottmeier, and J. H. Morison (1999), Ocean heat flux in the central Weddell Sea during winter, *J. Phys. Oceanogr.*, *29*, 1166–1179.
- Meier, W. N., and M. Dai (2006), High-resolution sea-ice motions from AMSR-E imagery, *Ann. Glaciol.*, *44*, 352–357.
- Meier, W. N., J. A. Maslanik, and C. W. Fowler (2000), Error analysis and assimilation of remotely sensed ice motion within an Arctic sea ice model, *J. Geophys. Res.*, *105*, 3339–3356.
- Muench, R. D., J. H. Morison, L. Padman, D. Martinson, P. Schlosser, B. Huber, and R. Hohmann (2001), Maud Rise revisited, *J. Geophys. Res.*, *106*, 2423–2440.
- Ou, H. W. (1991), Some effects of a seamount on oceanic flows, *J. Phys. Oceanogr.*, *21*, 1835–1845.
- Shaw, W. J., T. P. Stanton, J. H. Morison, and M. G. McPhee (2006), Observations of finestructure and mixing within a weakly stratified pycnocline during the MaudNESS experiment in the Weddell Sea, *Eos Trans. AGU*, *87*(36), Ocean Sci. Meet. Suppl., Abstract OS53H-0.
- Spreen, G., L. Kaleschke, and G. Heygster (2007), Sea ice remote sensing using AMSR-E 89 GHz channels, *J. Geophys. Res.*, *113*, C02S03, doi:10.1029/2005JC003384.
- L. de Steur, Norwegian Polar Institute, Hjalmar Johansens Gate 14, N-9296 Tromsø, Norway.
- R. Kwok, Jet Propulsion Laboratory, California Institute of Technology, 4800 Oak Grove Drive, Pasadena, CA 91109, USA.
- R. W. Lindsay, Polar Science Center, Applied Physics Laboratory, University of Washington, Seattle, WA 98105, USA.
- W. Meier, National Snow and Ice Data Center, University of Colorado, Boulder, CO 80309–0449, USA.